RESEARCH PAPER

A mixed-solvent strategy for facile and green preparation of graphene by liquid-phase exfoliation of graphite

Min Yi · Zhigang Shen · Shulin Ma · Xiaojing Zhang

Abstract A versatile and scalable mixed-solvent strategy, by which two mediocre solvents could be combined into good solvents for exfoliating graphite, is demonstrated for facile and green preparation of graphene by liquid-phase exfoliation of graphite. Mild sonication of crystal graphite powder in a mixture of water and alcohol could yield graphene nanosheets, which formed a highly stable suspension in the mixed solvents. The graphene yield was estimated as ~ 10 wt%. The optimum mass fraction of ethanol in water–ethanol mixtures and isopropanol in water–isopropanol mixtures was experimentally determined as ~ 40 and ~ 55 % respectively, which could be roughly predicted by the theory of Hansen solubility parameters. Statistics based on atomic force microscopic analysis show that up to ~ 86 % of the prepared nanosheets were less than 10-layer thick with a monolayer fraction of ~ 8 %. High resolution transmission electron microscopy, infrared spectroscopy, X-ray diffraction, and Raman spectrum analysis of the vacuum-filtered films suggest the graphene sheets to be largely free of defects and oxides. The proposed mixed-solvent strategy here extends the scope for liquid-phase processing graphene and gives researchers great freedom in designing ideal solvent systems for specific applications.

Keywords Graphene · Preparation · Liquid-phase exfoliation · Mixed-solvent strategy · Hansen solubility parameters

Introduction

Graphene has been fascinating researchers world-wide due to its unique physical and chemical properties and its hugely potential applications (Geim 2009; Geim and Novoselov 2007; Shapira et al. 2012). As a prerequisite of studying graphene and taking its related applications to the real world, methods for preparing graphene should be highly developed to make green, low cost and high-throughput graphene easily available. And developing green, low cost, and large-scale methods for producing graphene is always at the center of graphene research. Numerous routes have been proposed to prepare graphene (Dreyer et al. 2010; Novoselov et al. 2004; Norimatsu et al. 2011; Sun et al. 2010; Khan et al. 2010; Lotya et al. 2010; Hernandez et al. 2008; Bourlinos et al. 2009; Coleman 2009; Yi et al. 2011; Shen et al. 2011; Murugan et al. 2009; Valles et al. 2008; Stankovich et al. 2006), among which the reduction of graphene oxide in

M. Yi · Z. Shen (✉) · S. Ma · X. Zhang
Beijing Key Laboratory for Powder Technology Research & Development, Beijing University of Aeronautics and Astronautics, Beijing 100191, China
e-mail: shenzhg@buaa.edu.cn

Springer

liquid-phase has been a promising route to achieve mass production of graphene (Dreyer et al. 2010; Stankovich et al. 2006). However, this technique is a multistep process with severe oxidizer and reductant, and the residual defects cannot be removed completely (Dreyer et al. 2010; Stankovich et al. 2006). In addition, the direct liquid-phase exfoliation of crystal graphite assisted by sonication in certain solvents or solution makes facile, green, scalable, and low cost graphene production possible (Khan et al. 2010; Lotya et al. 2010; Hernandez et al. 2008; Bourlinos et al. 2009; Coleman 2009; Yi et al. 2011; Lu et al. 2009; Shen et al. 2011). But, currently the good solvents suitable for the sonication-assisted liquid-phase method are often high boiling, expensive, and toxic (Khan et al. 2010; Hernandez et al. 2008, 2010; Coleman 2009). Hence, there is definite room for improving liquid-phase production of graphene based on the exfoliation of crystal graphite. We will naturally raise a question that whether it is possible to find a green and low boiling solvent to reduce cost, eliminate pollution, and simplify the process of preparing graphene by sonication-assisted exfoliation. Supposing this expected solvent can be readily obtained or designed, the aim of preparing graphene with facility, scalability, low cost and no contamination could be achieved. The article here is aimed at finding or designing this kind of totally green solvents.

Unfortunately, the most common used and green solvents, water and alcohol, are conventionally deemed poor solvents for exfoliation and dispersion of graphene. Nevertheless, to the best of our knowledge, the theory of Hansen solubility parameters (HSP) has testified that a given solute can be dissolved in a designed mixture of even two nonsolvents (Hansen 2007). So it is desirable and possible to go further to achieve the aim of exfoliating crystal graphite into graphene in the water–alcohol mixture.

Herein, we report for the first time a mixed-solvent strategy for the facile and green preparation of graphene by exfoliating graphite in the water–alcohol mixture, where two kinds of alcohols, ethanol and isopropanol (IPA), were chosen for toxicological or hazardous considerations, and their exceptional advantages including low boiling point, low cost, and user-friendliness. And the nature of low boiling point allows quick solvents evaporation and individual graphene sheets easily sprayed cast onto substrates. By optimizing the mixing ratio of water and alcohol,

graphene dispersion with considerable concentration and high stability can be obtained. The demonstrated mixed-solvent strategy here is likely to expand the scope for exploiting solution-processable graphene and facilitate the manipulation of graphene toward different applications.

Experimental

Materials

The crystal graphite powder (particle sizes ≤ 300 mesh; purity ≥ 98.0 %), ethanol and IPA were purchased from Sinopharm Chemical Reagent Beijing Co., Ltd. The purified water was purchased from Beijing Kebaiao Biotech. Co., Ltd. All the materials employed in the experiments were used as received.

Preparation

Graphene dispersion was prepared by irradiating natural graphite powder in the fresh water–alcohol mixture with mild ultrasound, during which the mixing ratio of water and alcohol was varied. The true power output was estimated as ∼20 W by measuring the temperature rise of a known mass of water sonicated for various time (Supplementary Fig. S1). In the experiments of optimizing mixing ratio of water and alcohol, 20 mL solution in glass vessel with initial graphite concentration of 0.2 mg/mL was sonicated for 1 h in a fixed position in one sonic bath (KQ2200DE, 40 kHz, Kunshan Ultrasonic Instrument Co., Ltd., China). After sonicaton, the obtained dark dispersion was left to stand for 8 h for the sufficient sedimentation of large particles. Then the upper less dark dispersion was centrifuged at 1,000 and 3,000 rpm ($\times$112 and 1,008$\times g$) for 30 min with a 80-2 centrifuge (Jintan Zhongda Apparatus Co., Ltd, China) to remove any largish flakes, eventually resulting in homogeneous colloidal suspension of graphene sheets in the water–alcohol mixtures. For each specific mixture ratio, five samples were repeated. The concentration was determined after 1 Krpm centrifugation and standing for 2 weeks. The thin film for fourier transform infrared (FTIR) spectrum, Raman spectrum, and X-ray diffraction (XRD) analysis was prepared by vacuum filtration of the dispersion obtained from the above-mentioned

optimizing experiments through a porous membrane (mixed cellulose esters, pore size 0.22 µm).

Characterization

Height profile and morphology of graphene sheets were investigated with atomic force microscope (AFM) CSPM5500 (Being Nano-Instruments Ltd., China) equipped with a 13.56 µm scanner in tapping mode. AFM samples were prepared by pipetting several microliters graphene dispersion onto heating mica substrates which facilitated extremely quick evaporation of low boiling point solvents. Optical absorbance measurements were performed at 660 nm using a Vis spectrophotometer (721(E), Shanghai Spectrum Instruments Co., Ltd, China) with 1-cm cuvette. And the concentration C after centrifugation was determined from Lambert–Beer law, $A/l = \alpha C$, where α was taken as 2,460 mg/mL m^{-1} (Hernandez et al. 2008, 2010). Transmission electron microscopy (TEM) samples were prepared by pipetting a few microliters onto holey carbon mesh grid. TEM and high resolution TEM (HRTEM) imaging were performed by a JEOL JEM-2010FEF operated at 200 kV. Scanning electron microscopy (SEM) images were collected by a LEO 1530VP. SEM samples were prepared by recovering the pristine graphite powder, the precipitate after centrifugation, or the ruptured graphene films onto silicon substrates. XRD patterns of the graphene film were collected by using Cu Kα radiation ($\lambda = 1.5418$ Å) with an X-ray diffractometer (Bruke D8-advance) operating at 40 kV and 40 mA. Raman spectra were obtained directly from a thin graphene film deposited onto a glass slide by LabRAM HR800 excited with a 488 nm laser. Ten spectra were collected from different parts of the film. These spectra were then normalized to the G peak and averaged to give the Raman result presented here. FTIR spectrum of the filtered film was measured using a Nicolet iS10 spectrometer in the diffuse reflection mode. UV–Vis spectrum of the graphene dispersion was recorded on an Agilent-HP 8453 UV–Vis spectrometer.

Results and discussion

In the mixed-solvent strategy, it is natural for us to obtain the optimum mixing ratio of water and alcohol.

It is worth noting that the theory of HSP has been proved effective in studying the exfoliation and dispersion of graphene in solvents (Hernandez et al. 2010). A most useful concept that quantifies the principle of "like dissolves like" is the HSP distance (Ra) defined by $Ra = (4(\delta_{D1}-\delta_{D2})^2 + (\delta_{P1}-\delta_{P2})^2 + (\delta_{H1}-\delta_{H2})^2)^{1/2}$, where the idea is: the smaller the Ra, the better is the solubility (Hansen 2007). The details for calculating Ra are shown in the supporting information (Supplementary Table S1). The calculated and experimental results are shown in Fig. 1, in which the graphene concentration and Ra are strongly dependent on the mass fraction of alcohol in the mixture. For the water–ethanol mixture (W–E), the experimentally determined optimum mass fraction of ethanol is 40 %, which approaches the minimum point
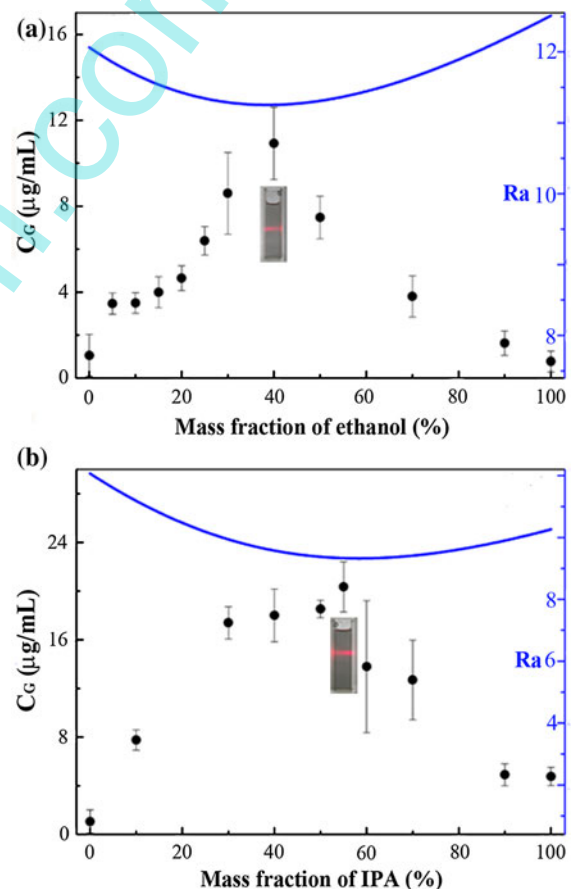

Fig. 1 Graphene concentration, C_G, and the calculated HSP distance, Ra, as a function of the mass fraction of ethanol (**a**) and IPA (**b**). C_G is shown as *dots* while Ra as *solid lines*. The Tyndall scattering effect is seen in the *inset* photographs for the graphene dispersion at the optimum concentration

(mass fraction of ~ 38.6 %) of Ra curve in Fig. 1a, indicating the consistence between the experimental results and theoretical prediction. At the optimum mixing ratio, the graphene concentration can reach 10.9 ± 1.7 µg/mL, ten times higher than that in single water or ethanol. Similarly, as shown in Fig. 1b, in the water–IPA mixture (W–IPA), the smallest Ra occurs at an IPA mass fraction of ~ 58.4 %, while the experimentally obtained optimum mixture consistently happens at an IPA mass fraction of ~ 55 %. The corresponding maximum graphene concentration is 20.4 ± 2.1 µg/mL, leading to a yield of ~ 10 wt% with an initial concentration of 200 µg/mL considered here. In short, the experimental results agree well with the trend of predictions made by HSP theory. The mixed solvents can achieve much higher concentration of graphene and turn mediocre solvents into effective ones.

Furthermore, we investigated the stability of graphene suspension in both two mixtures. The typical sedimentation curves are shown in Fig. 2. It has been addressed that the concentration during sedimentation is approximately amenable to first order exponential decay (Nicolosi et al. 2005), as shown in the inset equation of Fig. 2. The fitting details are presented in Supplementary Fig. S2 and Table S2. The values of C_0/C_I and time constant τ are ~ 67.4 %, ~ 129 h for W–E dispersion and ~ 80.2 %, ~ 139 h for W–IPA dispersion after 1 Krpm centrifugation, respectively. These values could be higher when higher

centrifugation speed, 3 Krpm, was utilized. The high C_0/C_I values indicate the appreciable stability of graphene suspension in the water–alcohol mixture with the vast majority of graphene remaining dispersed over long time scales, which can be comparable to that in good solvents such as N-methyl-pyrrolidone (Khan et al. 2010; Hernandez et al. 2008, 2010). So it is possible to enhance the stability of graphene dispersion by mixing mediocre solvents.

To assess the quality of graphene dispersion in the water–alcohol mixture, knowledge of the exfoliation degree, morphology feature, lateral size, and structural quality of the suspended graphene is indispensable. Once graphene can be dispersed and exfoliated, the ability to deposit individual flakes onto surfaces is very important for further characterization. This is problematic for graphene exfoliated in high boiling point solvents as their slow evaporation allows extensive reaggregation. However, our low boiling point solvent, alcohol and water, show advantages. Figures 3, 4 and Supplementary Figs. S3, S4 show some typical AFM and TEM images. The lateral dimension of most graphene sheets captured by AFM is between several hundred nanometers and several micrometers (Fig. 3a, b and Supplementary Figs. S3, S4) which is collaborated by the TEM results (Fig. 4a, b). Cross-sections of two typical graphene sheets in Fig. 3a, b show step heights of ~ 0.9 and ~ 0.57 nm, respectively, proving them to be monolayers or at most bilayers. Furthermore, based on statistical analysis of several hundred graphene sheets imaged by AFM, we can acquire the histogram of sheets thickness distribution as shown in Fig. 3c. It has been perceived that two-dimensional sheets are often raised by extra several angstroms above the supporting surface and monolayer graphene prepared by mechanical cleavage is more commonly observed with a thickness of ~ 1 nm by AFM (Novoselov et al. 2004). Even though the theoretical thickness of monolayer is 0.334 nm, height profile distortions generated by the AFM instrumental offset between the substrate and graphene sheet can result in differences of as much as 1 nm in the measured height of the very same graphene sheet (Nemesincze et al. 2008). Therefore, we can treat 0.4- to 1-nm thick sheets as monolayers which occupy ~ 6.7 % in W–E and ~ 8 % in W–IPA. Similarly, sheets no more than three layers (0.4- to 1.5-nm thick) can be estimated to account for ~ 35.8 % in W–E and ~ 39.3 % in W–IPA while few-layer
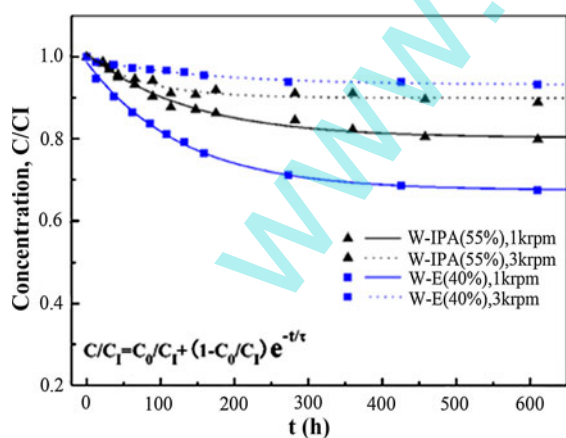

Fig. 2 Sedimentation curves of graphene dispersion at the optimum mixing ratio after 1 and 3 Krpm centrifugation. The *dots* correspond to the experimental data while the *dashed lines* are fitted by the *inset* equation

Fig. 3 Representative tapping mode AFM images (height scale 0–30 nm) of graphene sheets in W–E (**a**) and W–IPA (**b**). **c** A histogram of the frequency of nanosheets captured by AFM as a function of the thickness per nanosheet in W–E and W–IPA dispersion
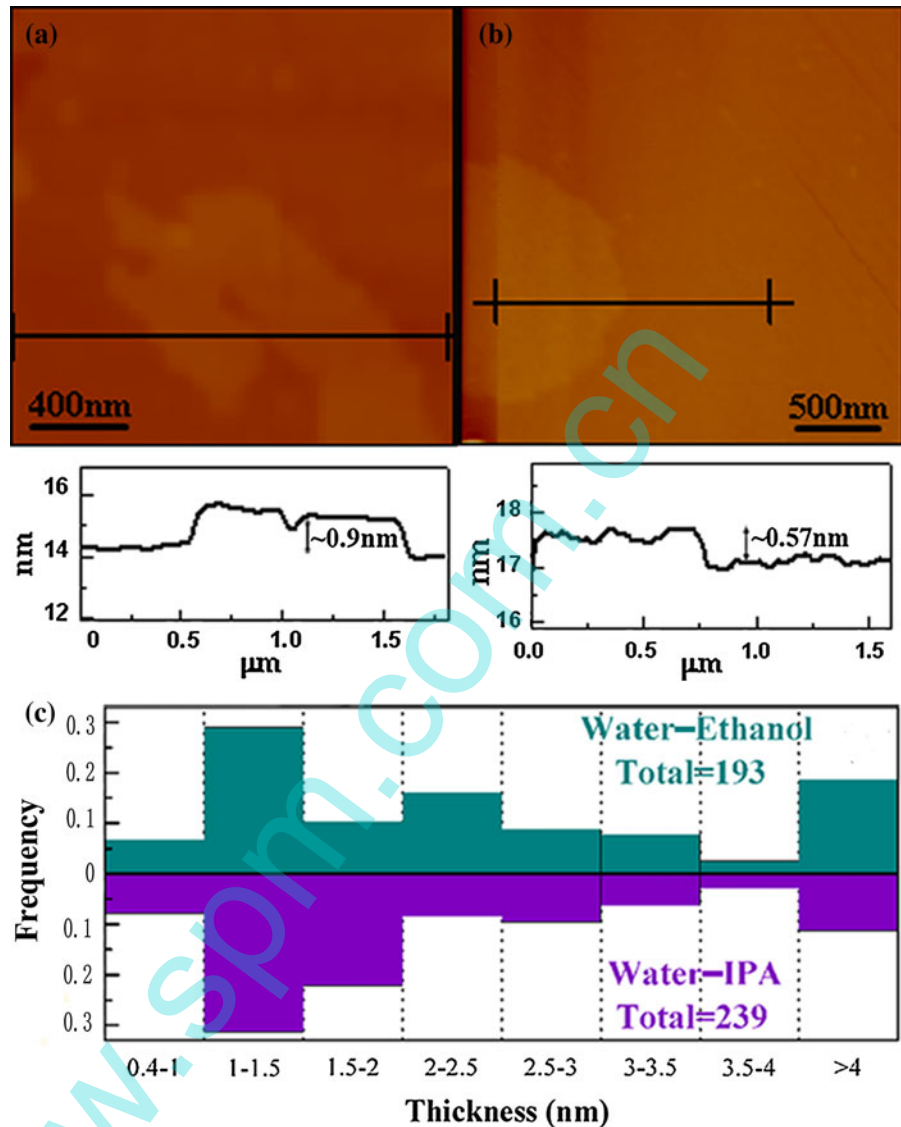
graphene (<10 layers) $\sim$78.8 % in W–E and $\sim$85.8 % in W–IPA. Thus, we believe that graphite in the water–alcohol mixture has been generally exfoliated into monolayer and few-layer graphene.

Shown in Fig. 4c is a HRTEM image of a graphene monolayer. The inset of Fig. 4c, a fast fourier transform (FFT) of this image which is equivalent to a diffraction pattern, shows a bright inner ring of {1100} spots and an extremely faint outer ring of {2110} spots. So the FFT here reveals the typical diffractions of the monolayer (Hernandez et al. 2008; Meyer et al. 2007). A filtered image of a square in Fig. 4c is presented in Fig. 4d, which is of atomic

resolution and clearly illustrates the hexagonal nature of the graphene. Moreover, intensity analysis along the line in Fig. 4d illustrates a C–C bond length of 1.47 Å (Fig. 4e) close to the theoretical value of 1.42 Å, and gives a hexagon width of 2.53 Å (Fig. 4f) coinciding with the expected value of 2.5 Å. In addition, all imaged regions exhibit this similar structure, indicating defect-free graphene and a non-destructive method.

In order to further characterize the graphene prepared here, films were cast onto porous membranes from water–alcohol dispersion by vacuum filtration. Typical SEM and AFM images of the filtered film are
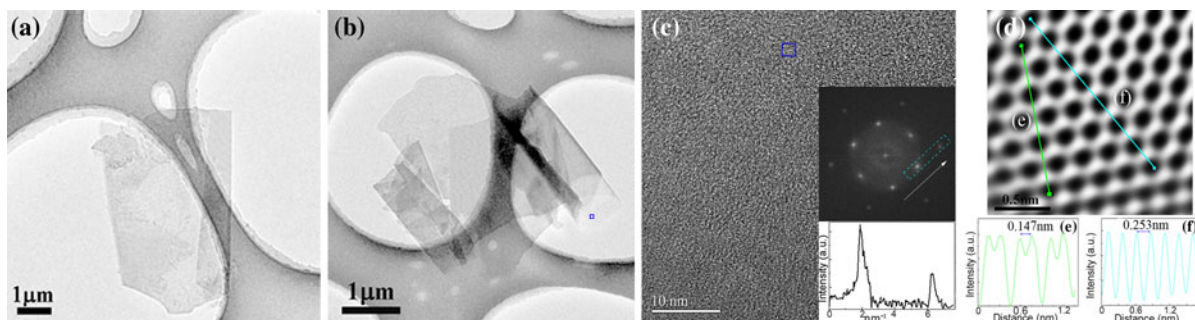
Fig. 4 Bright field TEM images of typical graphene sheets deposited from W–E (**a**) and W–IPA (**b**). **c** A HRTEM image of a section of a graphene monolayer indicated by a *square* in **b**. *Inset* FFT (equivalent to an electron diffraction pattern) of the image and the intensity distribution of spots in the *dotted-line rectangle*. **d** A filtered image (fourier mask filtering, twin-oval patter, edge smoothed by five pixels) of the *square* in **b**. Intensity analysis along the left line (**e**) and the right line (**f**)
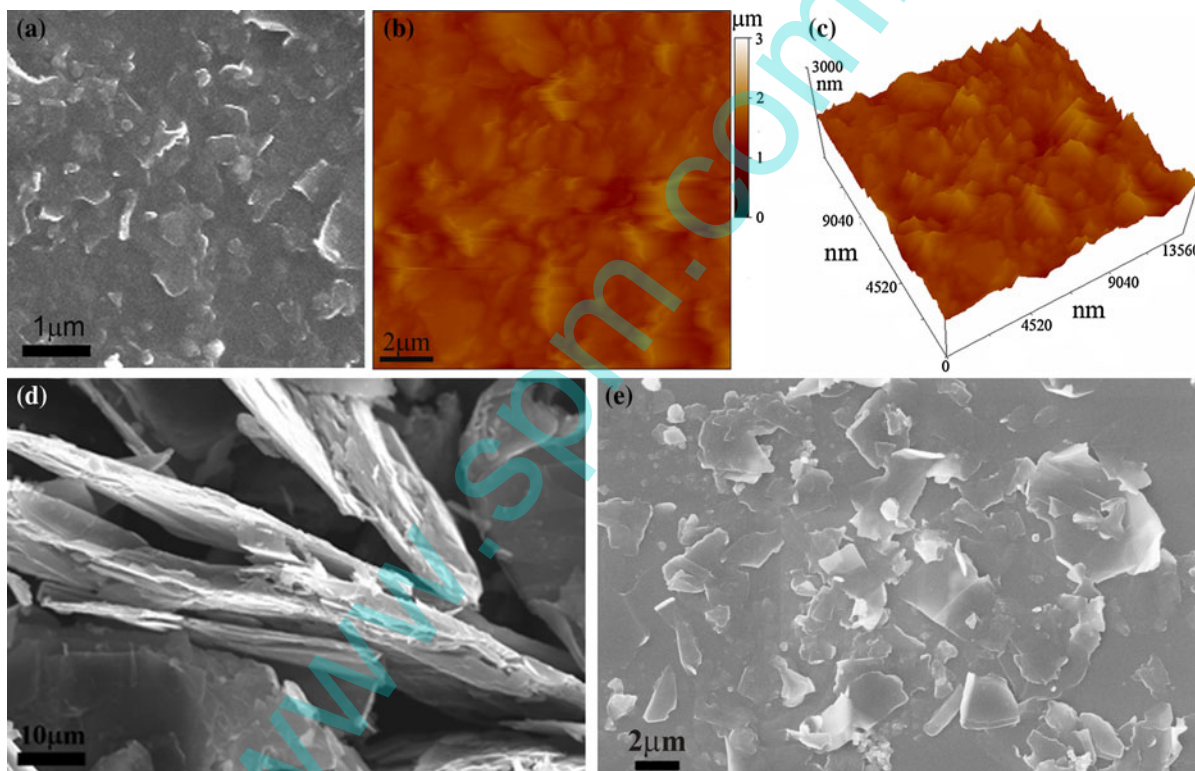

Fig. 5 A SEM image (**a**) and an AFM image (**b**) of a section of a filtered film. **c** 3D AFM image of (**b**). SEM images of graphite powder before sonication (**d**) and flakes after sonication recovered as a precipitate after centrifugation (**e**)

presented in Fig. 5a, b, c. The structural properties of graphene prepared here were characterized by UV–Vis spectroscopy, diffuse reflection FTIR spectrum, XRD, and Raman spectrum, as shown in Figs. 6 and 7. As expected for a quasi two-dimensional material, the UV–Vis spectrum in Fig. 6a is flat and featureless

(Abergel and Fal'ko 2007). The FTIR, XRD, and Raman spectra were investigated based on the filtered film. The diffuse reflection FTIR spectrum in Fig. 6b is virtually featureless. A key feature of the spectrum is the absence of peaks associated with C–O ($\sim 1,060$ cm^{-1}), C–OH ($\sim 1,340$ cm^{-1}), and –COOH

Fig. 6 **a** Typical UV–Vis absorption spectrum of graphene dispersed in W–E. **b** Diffusion reflection FTIR spectrum for the film filtered from water–alcohol dispersion
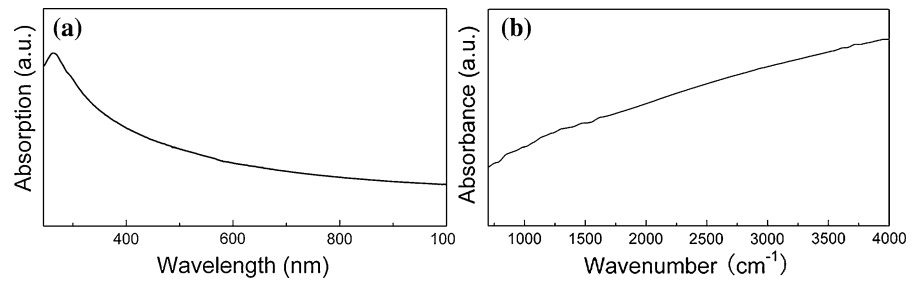
($\sim$1,710–1,720 cm^{-1}) groups (Titelman et al. 2005; Li et al. 2008a; Hontoria-Lucas 1995; Si and Samulski 2008), which are often prominently observable in films made from reduced graphene oxide (Whitby et al. 2011; Li et al. 2008a; Si and Samulski 2008) or chemically derived graphene (Li et al. 2008b). This indicates that we produce graphene rather than some form of graphene derivations, that our strategy does not chemically functionalized graphene, and that the filtered films are composed of largely defect-free material.

The collapse of cavitation bubbles induced by sonication in liquid can result in shock waves and shear waves to exfoliate thicker and larger graphite flakes into thinner and smaller sheets (Suslick and Price 1999; Shen et al. 2011; Cravotto and Cintas 2010), which is evidenced by SEM images before and after sonication, as shown in Fig. 5d, e. Therefore, considering remarkably thin graphene layers from high degree of exfoliation, the intensity of the (002) peak in the filtered film dramatically decreases and the corresponding FWHM increases due to Scherrer broadening (Morant 1970; Wilson et al. 2009), just as shown in Fig. 7a. In the inset of Fig. 7a, in contrast to graphite, no apparent peaks were detected in the XRD pattern for the filtered film, which may be attributed to the above-mentioned very thin flakes or graphene layers due to high degree of exfoliation. However, when the y-axis is changed to a logarithmic scale (Fig. 7a), a weak peak appeared at 2θ–26.6° corresponding to the (002) planes, which are identical to that in the graphite powder. This indicates an unchanged layer-to-layer distance in graphite. Nevertheless, no (004) peak can be detected for the filtered film, stating that the sublattices in the filtered film almost completely exclude the long-range order greater than four layer (Shih et al. 2011).

As for the Raman spectrum, in contrast to the graphite powder, the G band in the filtered film shifts
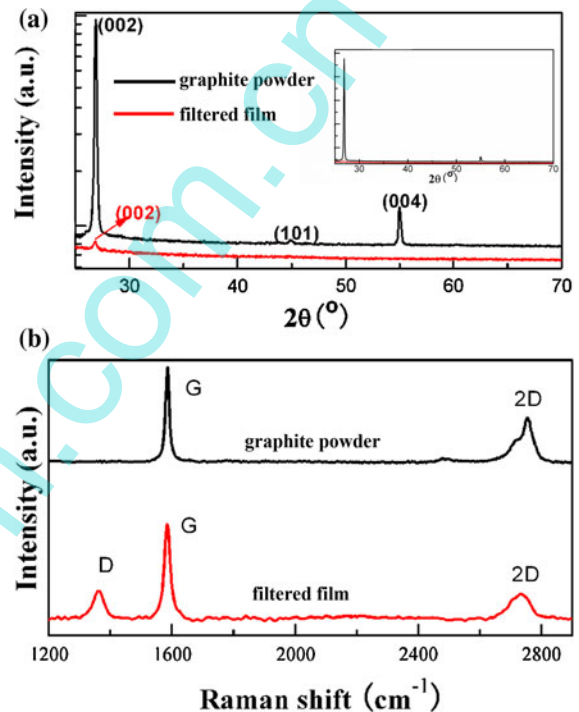

Fig. 7 **a** XRD spectra of the graphite powder and an as-filtered film with y-axis in a logarithmic scale. The FWHM of the (002) peak increased from $\sim$0.20° to $\sim$0.38°, and the (004) peak disappeared in the filtered film. *Inset* XRD spectra with y-axis in a linear scale. **b** Raman spectra of the graphite powder and an as-filtered film

to a slightly higher position ($\sim$2 cm^{-1}) while the 2D band to a lower position ($\sim$10 cm^{-1}) (Fig. 7b). This further supports that the graphite is exfoliated to single- or few-layer graphene (Malard et al. 2009). Both the structural disorder and edge defects can induce D bands, while the former can generally result in G bands' obvious broadening which is often found in the chemically reduced graphene (Stankovich et al. 2006, 2007). Meanwhile, the dynamic flow during the vacuum filtration may tear or fold micrometer sheets

into submicrometer ones, as shown in Fig. 5a. Consequently, seeing that the broadening of G band is unremarkable and the size of laser point (1–2 μm) used in the Raman system will inevitably cover the edges of graphene sheets in the filtered film, the D band in the filtered film may be largely attributed to the edge defects instead of the structural disorder. Also, the intensity ratio of I_D/I_G for the filtered film is ~ 0.3 which is much lower than that of the graphene oxide and chemically reduced graphene (Stankovich et al. 2006, 2007). Furthermore, as shown in Fig. 7b, the shape of 2D band in the filtered film is irrefutable evidence of few-layer graphene (Malard et al. 2009). Therefore, these imply that the filtered film is constituted of randomly (not Bernal) stacked graphene sheets, forming a disordered array of few-layer graphene (De et al. 2010).

Conclusions

In conclusion, we have demonstrated a mixed-solvent strategy for the green preparation of graphene by directly exfoliating crystal graphite powder in the water–alcohol mixture, achieving highly stabilized graphene dispersion with a graphene yield of ~ 10 wt%. And the optimum mixing ratio can be roughly predicted by the HSP theory, i.e., the optimum mass fraction of ethanol in W–E and W–IPA was determined as ~ 40 and ~ 55 %, respectively. The resulted graphene dispersion contains ~ 8 % monolayers and ~ 86 % few-layer graphene, where graphite lattice parameters remain and basal planes are largely free of structural disorder. The green nature of water, the lower toxicity of alcohol, the low cost and more accessible graphite powder, and the ease of operation make the demonstrated strategy facile, green, low cost, and potentially large-scale. Because the number of solvent mixtures is limitless, the mixed-solvent strategy allows researchers great freedom in designing ideal solvent systems for specific applications. It can be anticipated that the demonstrated mixed-solvent strategy will extends the scope for liquid-phase processing of graphene in green and user-friendly solution for broader applications.

References

Abergel DSL, Fal'ko VI (2007) Optical and magneto-optical far-infrared properties of bilayer graphene. Phys Rev B 75(15). doi:10.1103/PhysRevB.75.155430

Bourlinos AB, Georgakilas V, Zboril R, Steriotis TA, Stubos AK (2009) Liquid-phase exfoliation of graphite towards solubilized graphenes. Small 5(16):1841–1845. doi:10.1002/smll.200900242

Coleman JN (2009) Liquid-phase exfoliation of nanotubes and graphene. Adv Funct Mater 19(23):3680–3695. doi:10.1002/adfm.200901640

Cravotto G, Cintas P (2010) Sonication-assisted fabrication and post-synthetic modifications of graphene-like materials. Chemistry 16(18):5246–5259. doi:10.1002/chem.200903259

De S, King PJ, Lotya M, O'Neill A, Doherty EM, Hernandez Y, Duesberg GS, Coleman JN (2010) Flexible, transparent, conducting films of randomly stacked graphene from surfactant-stabilized, oxide-free graphene dispersions. Small 6(3):458–464. doi:10.1002/smll.200901162

Dreyer DR, Park S, Bielawski CW, Ruoff RS (2010) The chemistry of graphene oxide. Chem Soc Rev 39(1):228–240. doi:10.1039/b917103g

Geim AK (2009) Graphene: status and prospects. Science 324(5934):1530–1534. doi:10.1126/science.1158877

Geim AK, Novoselov KS (2007) The rise of graphene. Nat Mater 6(3):183–191. doi:10.1038/nmat1849

Hansen CM (2007) Hansen solubility parameters: a user's handbook. CRC Press, Boca Raton

Hernandez Y, Nicolosi V, Lotya M, Blighe FM, Sun Z, De S, McGovern IT, Holland B, Byrne M, Gun'Ko YK, Boland JJ, Niraj P, Duesberg G, Krishnamurthy S, Goodhue R, Hutchison J, Scardaci V, Ferrari AC, Coleman JN (2008) High-yield production of graphene by liquid-phase exfoliation of graphite. Nat Nanotechnol 3(9):563–568. doi:10.1038/nnano.2008.215

Hernandez Y, Lotya M, Rickard D, Bergin SD, Coleman JN (2010) Measurement of multicomponent solubility parameters for graphene facilitates solvent discovery. Langmuir 26(5):3208–3213. doi:10.1021/la903188a

Hontoria-Lucas C (1995) Study of oxygen-containing groups in a series of graphite oxides: physical and chemical characterization. Carbon 33(11):1585–1592. doi:10.1016/0008-6223(95)00120-3

Khan U, O'Neill A, Lotya M, De S, Coleman JN (2010) High-concentration solvent exfoliation of graphene. Small 6(7):864–871. doi:10.1002/smll.200902066

Li D, Muller MB, Gilje S, Kaner RB, Wallace GG (2008a) Processable aqueous dispersions of graphene nanosheets. Nat Nanotechnol 3(2):101–105. doi:10.1038/nnano.2007.451

Li X, Zhang G, Bai X, Sun X, Wang X, Wang E, Dai H (2008b) Highly conducting graphene sheets and Langmuir–Blodgett films. Nat Nanotechnol 3(9):538–542. doi:10.1038/nnano.2008.210

Lotya M, King PJ, Khan U, De S, Coleman JN (2010) High-concentration, surfactant-stabilized graphene dispersions. ACS Nano 4(6):3155–3162. doi:10.1021/nn1005304

Lu J, Yang JX, Wang J, Lim A, Wang S, Loh KP (2009) One-pot synthesis of fluorescent carbon nanoribbons, nanoparticles, and graphene by the exfoliation of graphite in ionic liquids. ACS Nano 3(8):2367–2375. doi:10.1021/nn900546b

Malard LM, Pimenta MA, Dresselhaus G, Dresselhaus MS (2009) Raman spectroscopy in graphene. Phys Rep 473(5–6):51–87. doi:10.1016/j.physrep.2009.02.003

Meyer JC, Geim AK, Katsnelson MI, Novoselov KS, Booth TJ, Roth S (2007) The structure of suspended graphene sheets. Nature 446(7131):60–63. doi:10.1038/nature05545

Morant RA (1970) The crystallite size of pyrolytic graphite. J Phys D Appl Phys 3(9):1367–1373. doi:10.1088/0022-3727/3/9/319

Murugan AV, Muraliganth T, Manthiram A (2009) Rapid, facile microwave-solvothermal synthesis of graphene nanosheets and their polyaniline nanocomposites for energy storage. Chem Mater 21(21):5004–5006. doi:10.1021/cm902413c

Nemesincze P, Osvath Z, Kamaras K, Biro L (2008) Anomalies in thickness measurements of graphene and few layer graphite crystals by tapping mode atomic force microscopy. Carbon 46(11):1435–1442. doi:10.1016/j.carbon.2008.06.022

Nicolosi V, Vrbanic D, Mrzel A, McCauley J, O'Flaherty S, McGuinness C, Compagnini G, Mihailovic D, Blau WJ, Coleman JN (2005) Solubility of $Mo_6S_{4.5}I_{4.5}$ nanowires in common solvents: a sedimentation study. J Phys Chem B 109(15):7124–7133. doi:10.1021/jp045166r

Norimatsu W, Takada J, Kusunoki M (2011) Formation mechanism of graphene layers on SiC (000$\bar{1}$) in a high-pressure argon atmosphere. Phys Rev B 84(3):1–6. doi:10.1103/PhysRevB.84.035424

Novoselov KS, Geim AK, Morozov SV, Jiang D, Zhang Y, Dubonos SV, Grigorieva IV, Firsov AA (2004) Electric field effect in atomically thin carbon films. Science 306(5696):666–669. doi:10.1126/science.1102896

Shapira P, Youtie J, Arora S (2012) Early patterns of commercial activity in graphene. J Nanopart Res 14(4). doi:10.1007/s11051-012-0811-y

Shen Z, Li J, Yi M, Zhang X, Ma S (2011) Preparation of graphene by jet cavitation. Nanotechnology 22(36):365306. doi:10.1088/0957-4484/22/36/365306

Shih CJ, Vijayaraghavan A, Krishnan R, Sharma R, Han JH, Ham MH, Jin Z, Lin S, Paulus GL, Reuel NF, Wang QH, Blankschtein D, Strano MS (2011) Bi- and trilayer graphene solutions. Nat Nanotechnol 6(7):439–445. doi:10.1038/nnano.2011.94

Si Y, Samulski ET (2008) Synthesis of water soluble graphene. Nano Lett 8(6):1679–1682. doi:10.1021/nl080604h

Stankovich S, Piner RD, Chen X, Wu N, Nguyen ST, Ruoff RS (2006) Stable aqueous dispersions of graphitic nanoplatelets via the reduction of exfoliated graphite oxide in the presence of poly(sodium 4-styrenesulfonate). J Mater Chem 16(2):155. doi:10.1039/b512799h

Stankovich S, Dikin DA, Piner RD, Kohlhaas KA, Kleinhammes A, Jia Y, Wu Y, Nguyen ST, Ruoff RS (2007) Synthesis of graphene-based nanosheets via chemical reduction of exfoliated graphite oxide. Carbon 45(7):1558–1565. doi:10.1016/j.carbon.2007.02.034

Sun Z, Yan Z, Yao J, Beitler E, Zhu Y, Tour JM (2010) Growth of graphene from solid carbon sources. Nature 468(7323):549–552. doi:10.1038/nature09579

Suslick KS, Price GJ (1999) Applications of ultrasound to materials chemistry. Annu Rev Mater Sci 29(1):295–326. doi:10.1146/annurev.matsci.29.1.295

Titelman GI, Gelman V, Bron S, Khalfin RL, Cohen Y, Bianco-Peled H (2005) Characteristics and microstructure of aqueous colloidal dispersions of graphite oxide. Carbon 43(3):641–649. doi:10.1016/j.carbon.2004.10.035

Valles C, Drummond C, Saadaoui H, Furtado CA, He M, Roubeau O, Ortolani L, Monthioux M, Penicaud A (2008) Solutions of negatively charged graphene sheets and ribbons. J Am Chem Soc 130(47):15802–15804. doi:10.1021/ja808001a

Whitby RLD, Korobeinyk A, Mikhalovsky SV, Fukuda T, Maekawa T (2011) Morphological effects of single-layer graphene oxide in the formation of covalently bonded polypyrrole composites using intermediate diisocyanate chemistry. J Nanopart Res 13(10):4829–4837. doi:10.1007/s11051-011-0459-z

Wilson NR, Pandey PA, Beanland R, Young RJ, Kinloch IA, Gong L, Liu Z, Suenaga K, Rourke JP, York SJ, Sloan J (2009) Graphene oxide: structural analysis and application as a highly transparent support for electron microscopy. ACS Nano 3(9):2547–2556. doi:10.1021/nn900694t

Yi M, Li J, Shen Z, Zhang X, Ma S (2011) Morphology and structure of mono- and few-layer graphene produced by jet cavitation. Appl Phys Lett 99(12):123112. doi:10.1063/1.3641863